[Article] DOI: 10.13208/j.electrochem.2219001 http://electrochem.xmu.edu.cn

Insight into the Effects of Cation Disorder and Surface Chemical Residues on the Initial Coulombic Efficiency of Layered Oxide Cathode

Jin-Li Liu[1,2], Han-Feng Wu[1,3], Zhi-Bei Liu[1], Ying-Qiang Wu[1*], Li Wang[1], Feng-Li Bei[2], Xiang-Ming He[1*]

(*1. Institute of Nuclear and New Energy Technology, Tsinghua University, Beijing 100084, P. R. China; 2. China National Quality Supervision Testing Center for Industrial Explosive Materials, Nanjing University of Science and Technology, Nanjing 210094, Jiangsu P.R. China; 3. School of Chemical & Environmental Engineering, China University of Mining and Technology (Beijing) , Beijing 100083, China*)

Abstract: Lithium layered oxide $LiNi_{0.6}Co_{0.2}Mn_{0.2}O_2$ (NCM622) is one of the most promising cathode materials in high-energy lithium-ion batteries for electric vehicles. However, one drawback for NCM622 is that its initial coulombic efficiency (ICE) is only about 87%, which is at least 6% lower than that of $LiCoO_2$ or $LiFePO_4$. In this work, we investigated the effects of surface chemical residues (e.g., LiOH and Li_2CO_3) and Li/Ni cation disorder resulted during the sintering on the ICE. We found that the ICE of the as-prepared samples could be boosted from 80.80% to 86.68% as the sintering temperatures were increased from 825 to 900 ℃. The corresponding Li/Ni cation disorder and surface chemical residues were also reduced with the increasing sintering temperatures. Furthermore, the ICE of the sample sintered at 825 ℃ could be enhanced by 3.57% after washing with HNO_3 solution to remove the surface residues despite the Li/Ni cation disorder being increased. These results demonstrate that minimizing the amount of surface residuals and the degree of Li/Ni cation disorder through an appropriate sintering process and post-treatment technology is critical to achieve a high ICE and improve the electrochemical performances of NCM622.

Key words: lithium layered oxide cathode; initial coulombic efficiency; surface chemical residues; Li/Ni cation disorder

1 Introduction

Pursuing high energy density lithium-ion batteries (LIBs) is one of the main trends in energy storage systems[1-5], while traditional $LiCoO_2$ (LCO) cathode is incapable of meeting the demand for future electric vehicle applications because of the bottleneck of limited capacity and high cost. To address these issues, Mn and Ni are commonly used to replace Co in the lithium layered metal oxide (i.e., $LiNi_{1-x-y}Co_xMnyO_2$, NCM)[6-12]. Hence, Ni-rich layered NCM622 cathode has become a great potential cathode material for high-energy LIBs due to its advantages with higher capacity (>180 $mAh \cdot g^{-1}$), lower cost, and improved cycling stability[13-17].

However, one main issue of the NCM622 cathode is the low initial coulombic efficiency (ICE) compared to LCO cathode (~95%)[18]. Low ICE means a largely irreversible capacity loss in the first charge-discharge process, in which more amount of anode (e.g., graphite) is needed to accept the irreversible Li^+, resulting in a

Cite as: Liu J L, Wu H F, Liu Z B, Wu Y Q, Wang L, Bei F L, He X M. Insight into the effect of cation disorder and surface chemical residues on the initial coulombic efficiency of layered oxide cathode. *J. Electrochem.*, 2022, 28(11): 2219001.

Received: 2022-08-21, Revised: 2022-09-27. *Corresponding author, Xiang-Ming He, E-mail: hexm@mail.tsinghua.edu.cn, Tel: (86-10) 62773274/62794226; Ying-Qiang Wu, E-mail: yqwu02@tsinghua.edu.cn, Tel: (86-10)89796078

dropping of the energy density[19-21]. The energy density of graphite||NCM battery dropped by about 3.5% if the ICE of NCM decreased from 95% to 87%. The low ICE is commonly believed to be from the cation disorder of Li/Ni in the crystalline structure[17, 22, 23] and the oxidation of electrolytes[18, 24]. Li/Ni cation disorder always occurs because of the similar radii of Ni^{2+} ion (0.69 Å) and Li^+ ion (0.76 Å), in which the Ni^{2+} ion in 3b sites can migrate to the 3a site of Li^+ during the sintering process[25]. As a result, the Ni^{2+} in the 3a site can block the diffusion of Li^+ during the Li^+ (de-)intercalation, leading to a low ICE and low-rate capability for Ni-rich NCM materials. To reduce the Li/Ni disorder, cation substitutions using Mg[26], Na[27], Zr[28], and Nb[29] have been investigated. Huang et al.[27] introduced Na^+ ion into the lithium layer to form $Li_{1-x}Na_xNi_{0.6}Co_{0.2}Mn_{0.2}O_2$, and an increased ICE from 83.3% to 86.2% was obtained as the degree of Li/Ni disorder lowered from 2.06% to 0.5%. However, a decreased ICE was reported when the Li/Ni cation disorder of a Ni-Rich $LiNi_{0.8}Co_{0.1}Mn_{0.1}O_2$ is reduced by doping of Ca^{2+}[23]. These controversial observations have not yet been fully understood.

Jo et al. [30] also reported a decrease ICE after re-heating the Ni-rich $LiNi_{0.7}Mn_{0.3}O_2$ materials, where the surface chemical residues (e.g., LiOH and Li_2CO_3) were increased during the sintering process. However, they did not further discuss the effects of residues. It is well accepted that LiOH can react with $LiPF_6$ to generate acidic HF in the electrolyte, while the decomposition of Li_2CO_3 can give rise to severe swelling upon storage at high temperatures[31, 32]. Both side reactions can lead to a decline in electrochemical performance, but their effect on ICE is rarely studied to the well of our knowledge. To study their effects, the content of surface chemical residues and Li/Ni cation disorder were finely measured and studied through the washing of samples in H_2O and/or HNO_3 solutions for NCM622. We found that ICE could be boosted after the washing, especially for the samples sintered at low temperate (e.g., 825 ℃), where the surface residues significantly affect the ICE compared with the Li/Ni cation disorder effect. These results demonstrate that minimizing the residual amount through an appropriate sintering process and post-treatment is critical to achieving high ICE and electrochemical performance for NCM622.

2 Experimental

2.1 Preparation of NCM622

$NiSO_4 \cdot 6H_2O$, $CoSO_4 \cdot 7H_2O$, and $MnSO_4 \cdot H_2O$ were mixed by a molar ratio of Ni:Co:Mn = 6:2:2 in distilled water (MSO_4, 2.0 mol·L^{-1}). The mixed solution was pumped into a continuous stirred tank reactor (CSTR, 2.0 L) under N_2 atmosphere[33]. At the same time, NaOH solution (10.0 mol·L^{-1}) and $NH_3 \cdot H_2O$ solution (10.0 mol·L^{-1}) were fed into the CSTR separately, where NH_3 acts as a chelating agent and the ratio of NH_3/MSO_4 was controlled at 0.8. The pH, temperature, and stirring speed were monitored and controlled carefully during the precipitation. After the precipitation, the suspension was stirred for another 24 h under N_2 atmosphere, then filtered, washed, and finally dried at 120 ℃ for 12 h. As-obtained $Ni_{0.6}Co_{0.2}Mn_{0.2}(OH)_2$ powder was mixed with $LiOH \cdot H_2O$ by a molar ratio of 1:1.05 and then sintered at 500 ℃ for 5 h, 800 ℃ for 5 h, and 825 ℃ (or 850, 875, 900 ℃ for other samples) for 6 h in air under a rising rate of 1 ℃·min^{-1}. Afterward, the product was slowly cooled to 800 ℃ for another 5 h, then to 500 ℃ with a drop rate of 1 ℃·min^{-1}.

2.2 Materials Characterizations and Electrode Preparation

The morphology of NCM622 was characterized by scanning electron microscope (SEM, Zeiss Merlin). X-ray diffraction (XRD, Bruker D8 ADVANCE) data were collected over a 2θ range of 10° ~ 80° with Cu-K_α radiation (λ = 1.5406 Å, 40 kV/40 mA). The XRD data were refined by the software of FullProf. The pH value was measured by an electronic pH meter (Fisher Scientific, Accumet AB15). TGA-DSC measurement was carried out by synchronous thermal analyzer (NETZSCH X70). X-ray photoelectron spectroscope (XPS, Thermofisher ESCALAB 250Xi) was employed using an Al K_α source (1487 eV). The NCM622 electrode was prepared as below. NCM622 powder, acetylene black, and poly

(vinylidene fluoride) (PVDF) were mixed with a mass ratio of 90:4:6 in N-methyl pyrrolidinone (NMP) for 20 min using a Thinky mixer to obtain a uniform slurry. The slurry was then cast on an aluminum foil to form the NCM622 electrode. The electrode was dried at 120 ℃ in a vacuum oven overnight and roll-pressed before use. The loading density of the active materials (i.e., cathode powder) was controlled at around 8.5 mg·cm^{-2}.

2.3 Electrochemical Measurements

The electrochemical measurements were performed using a 2032-type coin cell, in which the counter lithium anode and the separator of Celgard 2320 were used. The electrolyte was 1.0 mol·L^{-1} $LiPF_6$ in EC/ EMC (3:7 by weight) with 2wt% VC as an additive. The cell was assembled in an argon-filled glovebox, where the contents of O_2 and H_2O were strictly maintained below 1.0 ppm. The cut-off voltage was controlled at 3.0 ~ 4.3 V (vs. Li/Li$^+$), and the galvanostatic charge/discharge curves were recorded by the Neware instrument.

3 Results and Discussion

TGA-DSC analysis curves of $Ni_{0.6}Co_{0.2}Mn_{0.2}(OH)_2$ and $LiOH·H_2O/Ni_{06}Co_{02}Mn_{02}(OH)_2$ mixture are shown in Figure 1. For the $Ni_{0.6}Co_{0.2}Mn_{0.2}(OH)_2$, the weight loss of 1.18% at 200 ℃ belonged to the loss of adsorbed water (Figure 1a and 1c). The larger weight loss (12.85%) near 300 ℃ could be ascribed to the thermal decomposition of $Ni_{0.6}Co_{0.2}Mn_{0.2}(OH)_2$ to oxides[33]. Differently, the weight loss (14.07%) at 200 ℃ observed (Figure1b and 1d) for the $LiOH·H_2O/Ni_{0.6}Co_{0.2}Mn_{0.2}(OH)_2$ mixture was due to the loss of crystallization water from $LiOH·H_2O$, and the thermal decomposition of $Ni_{0.6}Co_{0.2}Mn_{0.2}(OH)_2$ occurred at

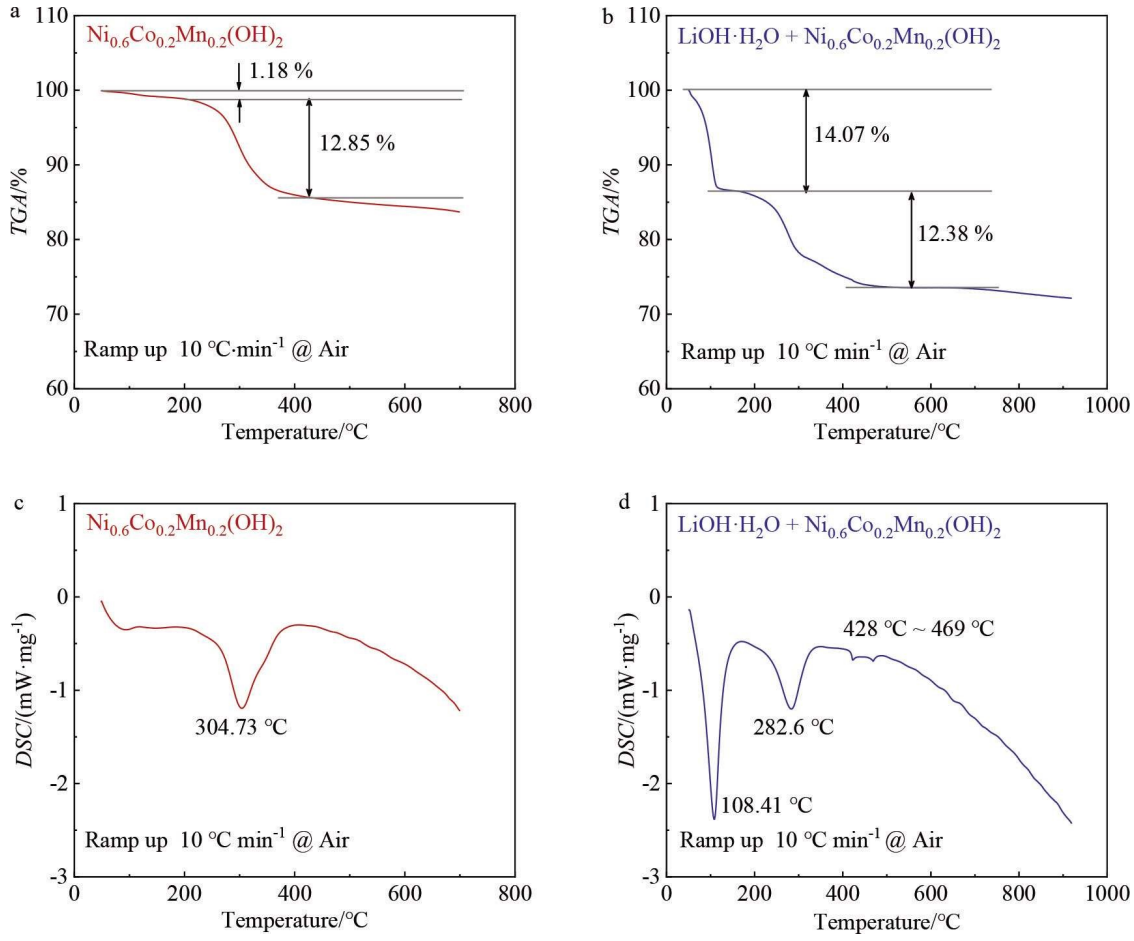

Figure 1 TGA-DSC curves of $Ni_{0.6}Co_{0.2}Mn_{0.2}(OH)_2$ (a, c) and $LiOH·H_2O/Ni_{0.6}Co_{0.2}Mn_{0.2}(OH)_2$ mixture (b, d). The TAG-DSC tests were under air atmosphere with a ramp-up rate of 10 ℃·min^{-1}. (color on line)

282.6 ℃. In addition, two peaks of heat release were observed between 428 and 469 ℃, which was attributed to the lithiation of the sample (Figure 1d). Thus, a pre-lithiation was carried out at 500 ℃ for 5 h before the sintering at high temperature (> 825 ℃) to reduce the evaporation of lithium salt.

The SEM images of the NCM 622 samples sintered at 825, 850, 875 and 900 ℃ are shown in Figure 2a-d. All the samples present a sphere-like morphology with a particle size of around 10 μm. The

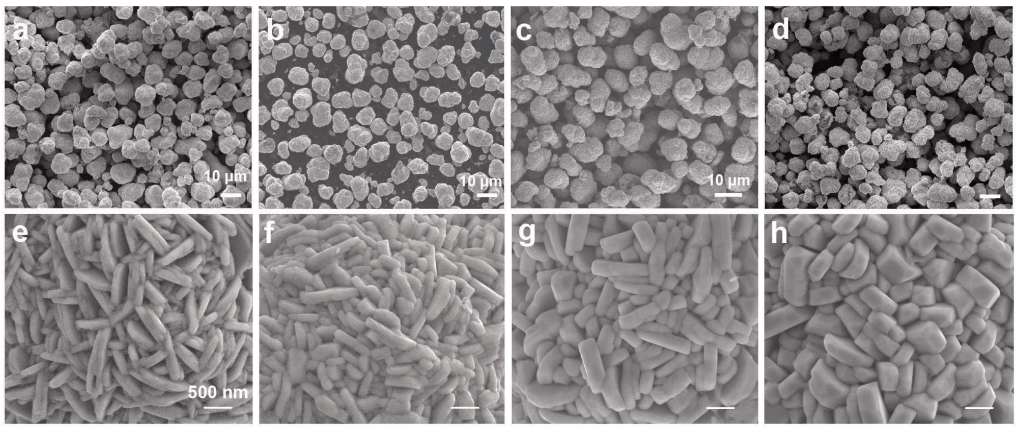

Figure 2 SEM images of the NCM622 materials sintered at different temperatures: (a, e) 825 ℃, (b, f) 850 ℃, (c, g) 875 ℃ and (d, h) 900 ℃.

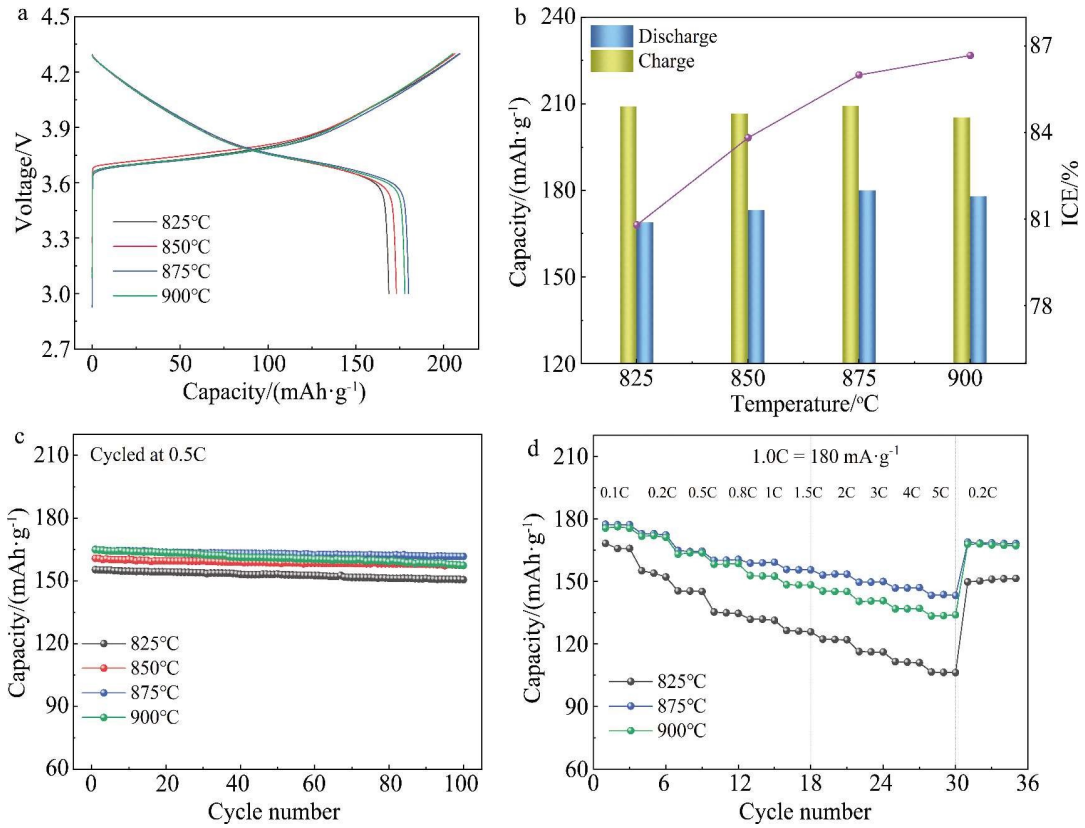

Figure 3 (a) The initial charge/discharge curves of NCM622 cathodes sintered at different temperatures under 0.1C, where 1.0 C = 180 mA·g^{-1}. (b) A comparison of the ICE and charge/discharge capacity. (c) The cycling performance of the electrodes under 0.5C. And (d) the rate capabilities of the 825, 875 and 900 ℃ sintered samples. (color on line)

high-resolution SEM images in Figure 2e-h show that the primary particle becomes thicker along with the [001] crystal axis with the sintered temperature increasing. This morphologic structure evolution would lead to an increase in the active planes area, and thus the improved electrochemical performance[34, 35].

Figure 3a shows the initial charge/discharge curves of the NCM622 cathode sintered at different temperatures. The ICE increased from 80.80% to 86.68% when the sintering temperature increased from 825

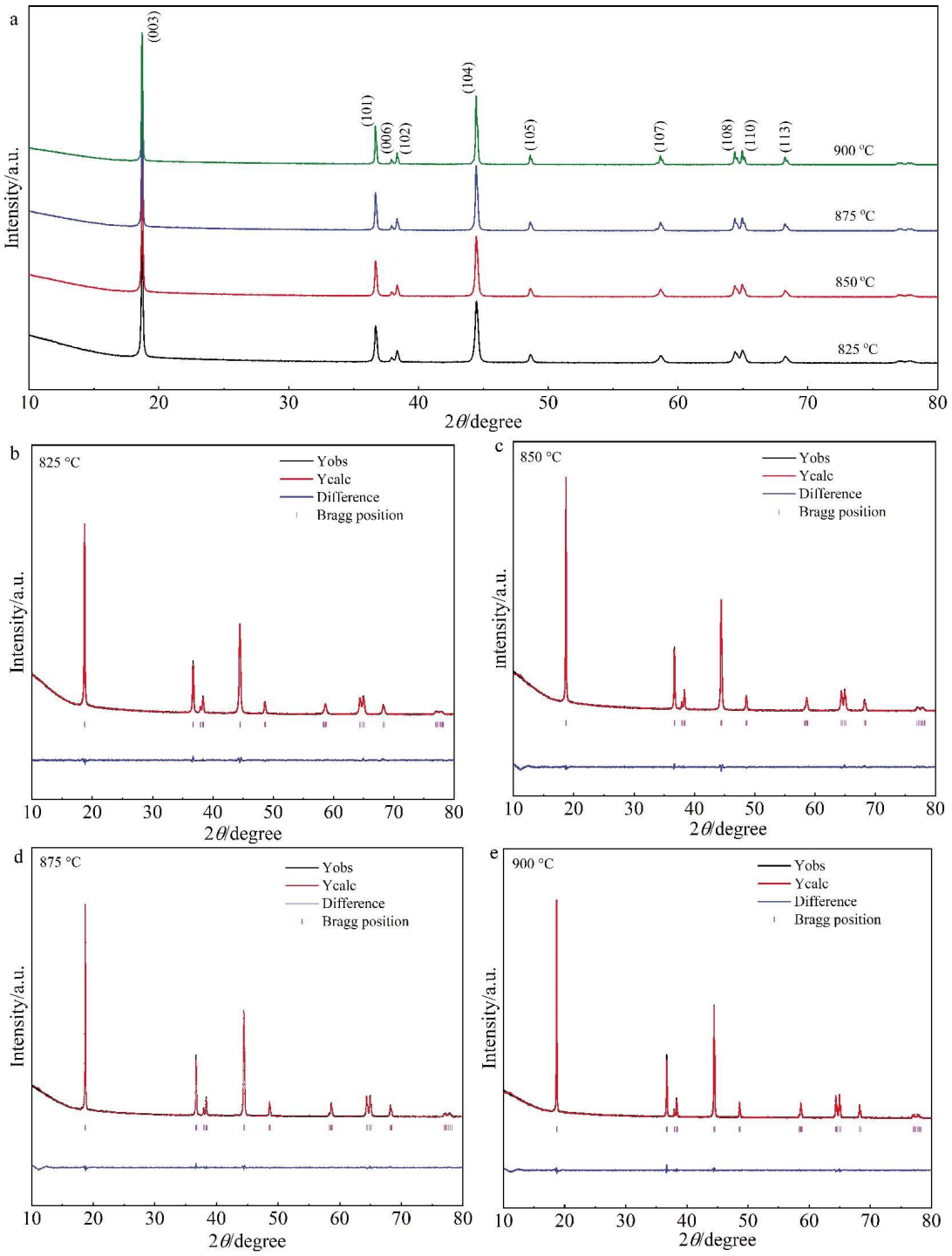

Figure 4 (a) XRD plots of the NCM622 materials sintered at different temperatures. The Rietveld refinement from the XRD data of samples sintered at (b) 825 ℃, (c) 850 ℃, (d) 875 ℃ and (e) 900 ℃. (color on line)

℃ to 900 ℃ (Figure 3b). We found that there was no obvious difference in the charge capacity while the discharge capacity increased significantly from 168.89 to 178.0 mAh·g^{-1}. These results revealed that the effect of charge capacity from the electrolyte oxidation could be ignored and thus it had no obvious effect on the low ICE under 4.3 V (vs. Li/Li$^+$). The cycling performance and the rate capability of the samples are shown in Figure 3c-d. The sample sintered at 875 ℃ exhibited the best rate capability and cycling stability. A high capacity of 165.0 mAh·g^{-1} was obtained at 0.5C with the capacity retention of 98.0% (i.e., 161.7 mAh·g^{-1}) over 100 cycles (Figure 3c). The rate capacities of the 875 ℃ sintered sample were 5.4%, 11.4%, 13.4%, 18.3%, 20.4%, 23.1%, 25.1%, 28.5%, 31.6% and 34.4% higher than those of the 825 ℃ sintered sample (Figure 3d). These values were also 1.0%, 0.7%, 1.1%, 1.2%, 3.9%, 4.9%, 5.3%, 6.5%, 7.3% and 7.4% higher than those of the sample sintered at 900 ℃.

To analyze the ICE and electrochemical performance, the structures of NCM622 sintered at different temperatures were studied. The XRD analysis demonstrated that all the samples have a layered structure (α-$NaFeO_2$) with a space group of $R\bar{3}m$, where the split of (108) and (110) peaks became more obvious (Figure 4a). This revealed the crystallinity and layered characteristic increased as rising the sintering temperature[36]. The XRD data were further refined by the software of FullProf (Figure 4b-e) to obtain the content of Li/Ni cation disorder for the NCM622 samples (Figure 5a). The results showed that the content of Li/Ni cation disorder decreased with the sintering temperature increasing from 825 ℃ to 900 ℃, where the Li/Ni disorder was decreased from 2.86% to 1.90% (Figure 5a). This variation trend confirmed that the less Li/Ni disorder in the material, the higher the ICE. Note that there was a slight increase in the lattice parameters (Table 1). This is because the smaller Ni^{2+} (0.69 Å) occupied the Li^+(0.76 Å) site in the Li layers, rendering the lattice expansion, which was good for the Li^+ migration[30], and then is responsible for the improved electrochemical performance for the sample sintered at 875 ℃.

Furthermore, the surface chemical residues (e.g., LiOH and Li_2CO_3) were expressed by the pH value which was measured by dispersing 10wt% of the NCM622 powder in water, and higher pH means more content of the surface chemical residues. The surface chemical residues were formed through the reactions of Li_2O with CO_2 (i.e., $Li_2O + CO_2 \rightarrow Li_2CO_3$) and H_2O molecules (i.e., $Li_2O + H_2O \rightarrow 2LiOH$) in air during the cooling process[30]. We found that the pH value also decreased from 11.49 to 11.40 with increasing the sintering temperature (Figure 5b). To distinguish the effects of the Li/Ni disorder and surface chemical residues on the ICE, the sample sintered at 825 ℃ was washed with water or diluted HNO_3 solution to remove the surface chemical residues. Figure 5c-d compare the high-resolution SEM images of the samples before and after the water washing. A clean and smooth surface of the particle after the washing indicates that the surface chemical residues were removed (Figure 5d). XPS characterization was conducted to analyze the surface structure of the sample before and after washing with HNO_3 solution (Figure 6). Before the washing, the peaks at 855.5 eV, 854.5

Table 1 Cell parameters and cation disorder of $Li_{1-x}Ni_xNi_{0.6-x}Li_xCo_{0.2}Mn_{0.2}O_2$ at different sintering temperatures.

T (℃)	a (Å)	b (Å)	c (Å)	V (Å^3)	c/a	Li/Ni disorder (%)	R_{wp} (%)	R_{exp} (%)	Chi^2
800	2.86875	2.86875	14.22397	101.3764	4.95825	2.712	7.30	5.27	1.92
825	2.86907	2.86907	14.22614	101.4143	4.95845	2.856	7.19	5.37	1.80
850	2.86918	2.86918	14.22696	101.3764	4.95855	2.568	7.89	5.15	2.35
875	2.86944	2.86944	14.22756	101.4504	4.95831	2.436	8.14	5.09	2.56
900	2.86944	2.86944	14.22770	101.4514	4.95835	1.896	7.89	4.90	2.59

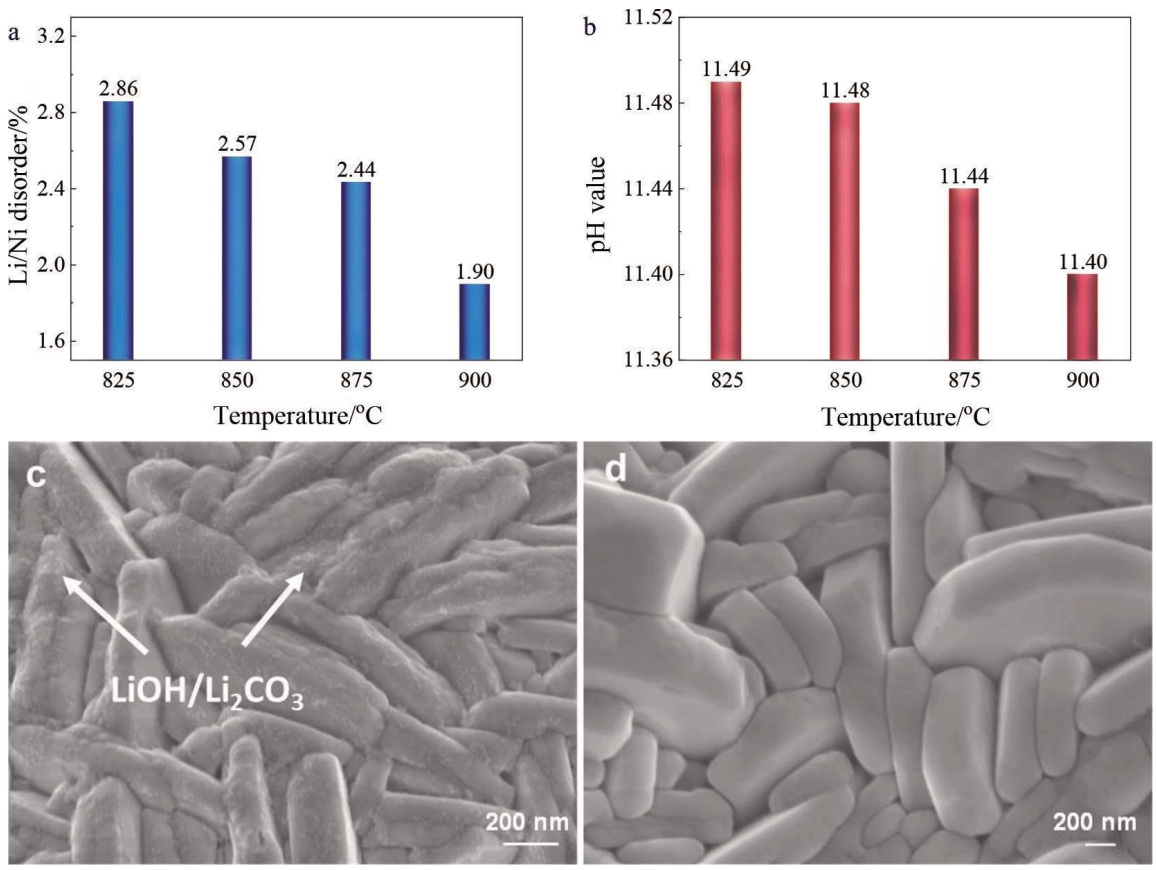

Figure 5 (a) The Li/Ni cation disorder plot obtained from the Rietveld refinement. (b) The pH value plot of the powder materials. High-resolution SEM images of the 825 °C sintered sample (c) before and (d) after washing with water. (color on line)

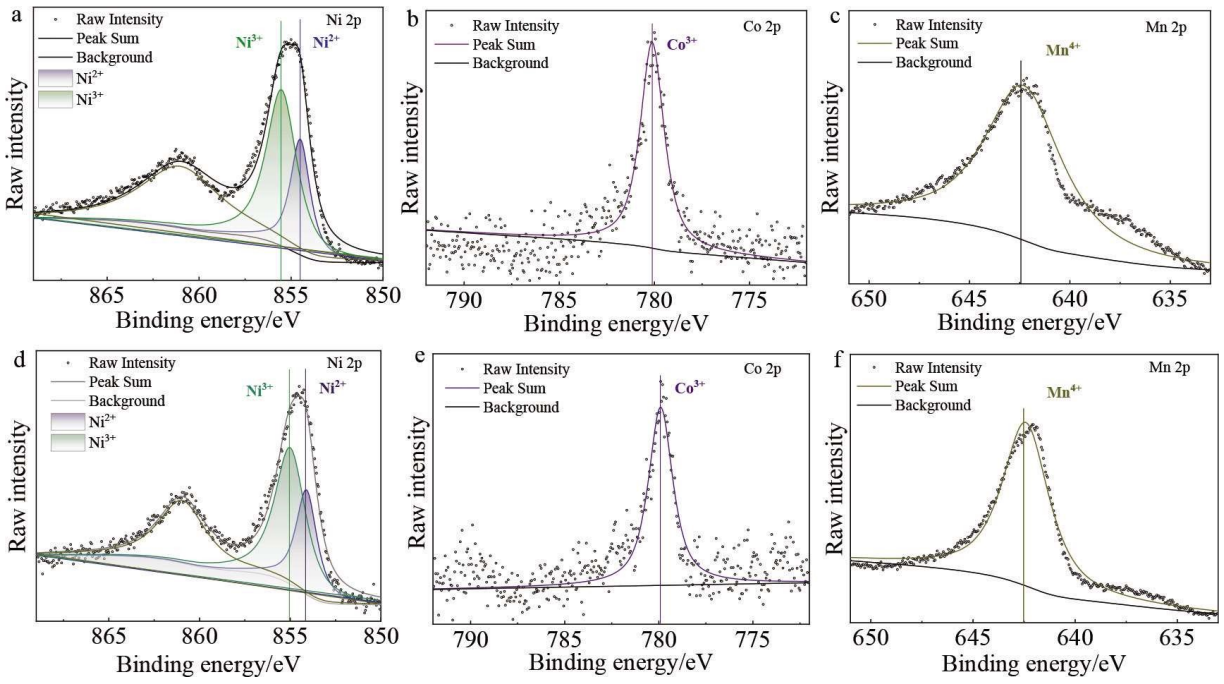

Figure 6 XPS spectra of Ni 2p, Co 2p, Mn 2p of the 825 °C sintered sample (a-c) before and (d-f) after washing with HNO_3 solution. (color on line)

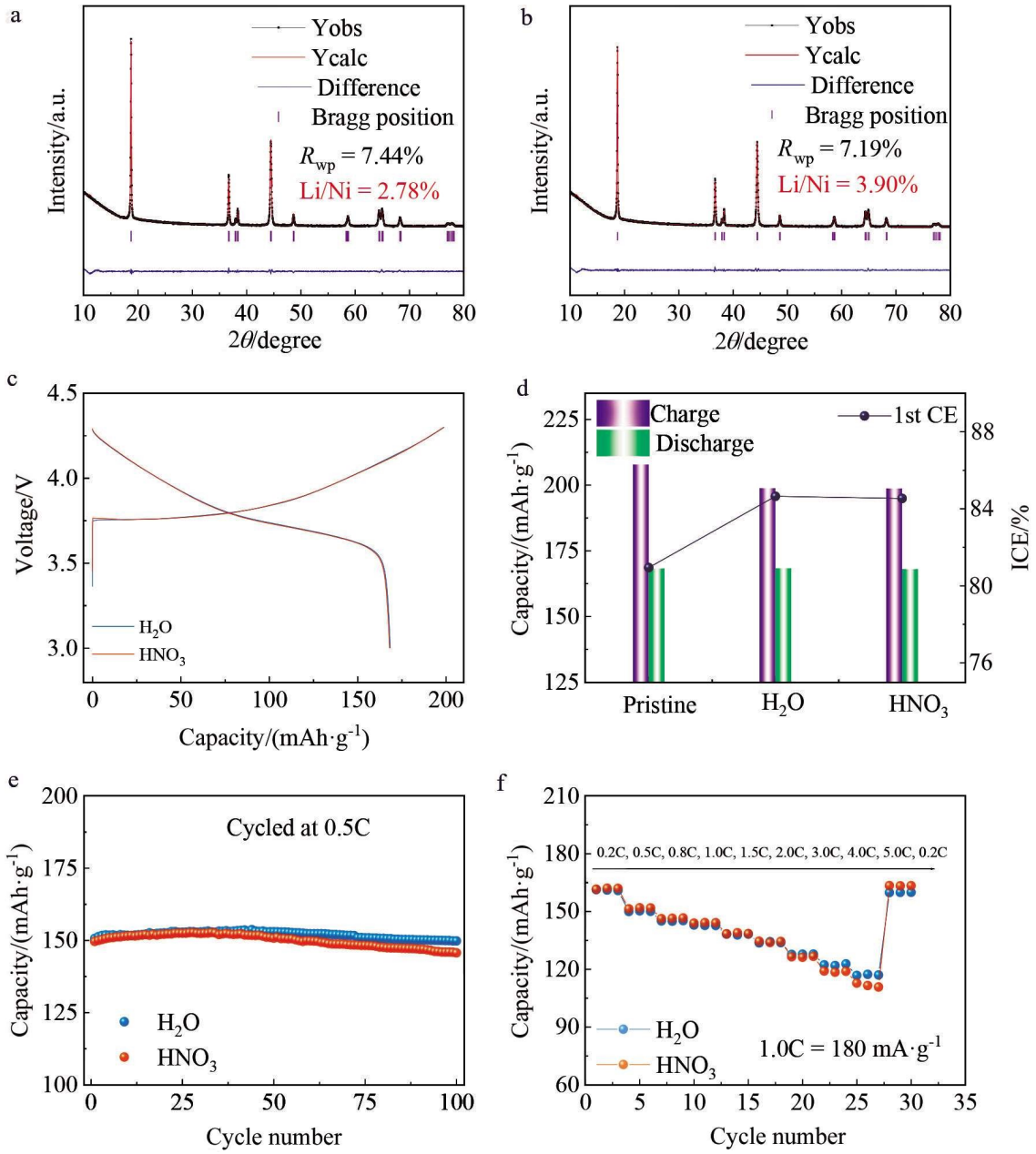

Figure 7 The Rietveld refinement plots from the XRD data of the samples washed by (a) H_2O and (b) HNO_3 solution (0.15 mol·L^{-1}). (c) The initial charge/discharge curves of the 825 ℃ sintered sample washed with water and HNO_3 under 0.1C. (d) Charge/discharge capacity and the ICE plots. (e) The cycling performance and (f) rate capability of the 825 ℃ sintered samples washed with water and HNO_3 solution. (color on line)

eV, 780.1 eV, and 642.3 eV were attributed to Ni^{3+}, Ni^{2+}, Co^{3+}, and Mn^{4+} in $LiNi_{0.6}Co_{0.2}Mn_{0.2}O_2$, respectively[37-40] (Figure 6a-c). We found that the valence of the transition metal elements was not altered after the washing (Figure 6d-f).

Thus, several interesting results can be further summarized: i) Li/Ni cation disorder decreased a little bit from 2.86% to 2.78% after H_2O washing for the sample sintered at 825 ℃ (Figure 7a), and the ICE increased to 84.65% (Figure 7d), which was 3.7% higher than that of the pristine sample; ii) alternatively, the cation disorder increased to 3.9% after HNO_3 solution washing (Figure 7b), but the ICE could still increase to 84.54% (Figure 7d), which was about

3.59% higher than that of the pristine; iii) the discharge capacity almost had no obvious change (~168 mAh·g^{-1}), but the charge capacity decreased from 207.9 mAh·g^{-1} to 198.8 mAh·g^{-1} (Figure 7c-d); iv) the capacity retention values of pristine NCM622 electrode, and washed by H_2O and by HNO_3, were 95.6%, 99.4% and 97.4% after 100 cycles, respectively (Figure 7e); v) the rate capacities of H_2O washed sample were 3.4%, 8.4%, 9.3%, 9.7%, and 10.2% higher than those of the pristine sample at 0.5C, 1.0C, 2.0C, 4.0C and 5.0C, respectively. Even for the HNO_3 washed sample with the increased cation disorder, it could still exhibit increased capacities of 4.1%, 9.2%, 10.1%, 6.8%, and 5.9% over those of pristine sample under the same variation of C rate (Figure 7f).

Our results confirmed that the removal of chemical residues from the samples could minimize the aforementioned side-reactions during the charging process. More importantly, it also means that the surface residues can affect the ICE, thus its amount becomes a crucial role to determine the performance as that of the Li/Ni cation disorder. We found that the ICE could still be increased by 3.6% despite the increased Li/Ni cation disorder after washing with HNO_3 solution. In this way, we can summarize that minimizing the surface residues through an appropriate temperate is critical to achieving a high ICE and improving electrochemical performance.

4 Conclusions

In summary, the uniform and spherical NCM622 cathode materials were synthesized by co-precipitation method. The effects of Li/Ni cation disorder and surface chemical residues on the ICE and electrochemical performance were studied in detail with varying sintering temperatures and post-treatment. We found that the ICE increased from 80.8% to 86.7% as increasing the thermal-treating temperature from 825 to 900 ℃, and high performance could be obtained at 875 ℃. More importantly, we confirmed that the surface chemical residues affect the ICE significantly, especially for the samples sintered at a low temperature. Our results interpreted the reason why higher performance could be obtained at the temperature of 875 ℃, under which the surface chemical residues, Li/Ni cation disorder, and crystallinity can be optimized through an appropriate sintering condition for high ICE and electrochemical performance.

Acknowledgements:

This work is supported by the National Natural Science Foundation of China (No. U21A20170), and the Ministry of Science and Technology of China (No. 2019YFE0100200, 2019YFA0705703, and 2021YFB2501900).

References:

[1] Wu Y Q, Xie L Q, Ming H, Guo Y J, Hwang J Y, Wang W X, He X M, Wang L M, Alshareef H N, Sun Y K, Ming J. An empirical model for the design of batteries with high energy density[J]. ACS Energy Lett., 2020, 5(3): 807-816.

[2] Zhang B, Wang L, Zhang H, Xu H, He X M. Revelation of the transition-metal doping mechanism in lithium manganese phosphate for high performance of lithium-ion batteries[J]. Battery Energy, 2022, 1(4): 20220020.

[3] Xue H J, Wu Y Q, Zou Y G, Shen Y B, Liu G, Li Q, Yin D M, Wang L M, Ming J. Unraveling metal oxide role in exfoliating graphite: new strategy to construct high-performance graphene-modified SiO_x-based anode for lithium-ion batteries[J]. Adv. Funct. Mater., 2020, 30(21): 1910657.

[4] Wu Y Q, Ming H, Li M L, Zhang J L, Wahyudi W, Xie L Q, He X M, Wang J, Wu Y P, Ming J. New organic complex for lithium layered oxide modification: ultrathin coating, high-voltage, and safety performances[J]. ACS Energy Lett., 2019, 4(3): 656-665.

[5] Zhang B, He Y F, Gao H Q, Wang X D, Liu J L, Xu H, Wang L, He X M. Unraveling the doping mechanisms in lithium iron phosphate[J]. Energy Mater., 2022, 2: 200013.

[6] Li W D, Dolocan A, Oh P, Celio H, Park S, Cho J, Manthiram A. Dynamic behaviour of interphases and its implication on high-energy-density cathode materials in lithium-ion batteries[J]. Nat. Commun., 2017, 8: 14589.

[7] Ryu H H, Park K J, Yoon C S, Sun Y K. Capacity fading of Ni-rich $Li[Ni_xCo_yMn_{1-x-y}]O_2$ ($0.6 \leqslant x \leqslant 0.95$) cathodes for high-energy-density lithium-Iion batteries: bulk or surface degradation?[J]. Chem. Mater., 2018, 30(3): 1155-1163.

[8] Wu Y Q, Xie L Q, He X M, Zhuo L H, Wang L M, Ming J. Electrochemical activation, voltage decay and hysteresis of Li-rich layered cathode probed by various cobalt content[J]. Electrochim. Acta, 2018, 265: 115-120.

[9] Fan L, Wei S Y, Li S Y, Li Q, Lu Y Y. Recent progress of

the solid-state elect rolytes for high-energy metal-based batteries[J]. Adv. Energy Mater., 2018, 8(11): 1702657.

[10] Wu Y Q, Ming J, Zhuo L H, Yu Y C, Zhao F Y. Simultaneous surface coating and chemical activation of the Li-rich solid solution lithium rechargeable cathode and its improved performance[J]. Electrochim. Acta, 2013, 113: 54-62.

[11] Jun D W, Yoon C S, Kim U H, Sun Y K. High-energy density core-shell structured $Li[Ni_{0.95}Co_{0.025}Mn_{0.025}]O_2$ cathode for lithium-ion batteries[J]. Chem. Mater., 2017, 29 (12): 5048-5052.

[12] Lee W, Muhammad S, Kim T, Kim H, Lee E, Jeong M, Son S, Ryou J H, Yoon W S. New insight into Ni-rich layered structure for next-generation Li rechargeable batteries[J]. Adv. Energy Mater., 2018, 8(4): 1701788.

[13] Liu W, Li X F, Xiong D B, Hao Y C, Li J W, Kou H R, Yan B, Li D J, Lu S G, Koo A, Adair K, Sun X L. Significantly improving cycling performance of cathodes in lithium ion batteries: the effect of Al_2O_3 and $LiAlO_2$ coatings on $LiNi_{0.6}Co_{0.2}Mn_{0.2}O_2$[J]. Nano Energy, 2018, 44: 111-120.

[14] Lee S W, Kim M S, Jeong J H, Kim D H, Chung K Y, Roh K C, Kim K B. Li_3PO_4 surface coating on Ni-rich $LiNi_{0.6}Co_{0.2}Mn_{0.2}O_2$ by a citric acid assisted sol-gel method: improved thermal stability and high-voltage performance [J]. J. Power Sources, 2017, 360: 206-214.

[15] Chen Z Q, Wang J, Huang J X, Fu T, Sun G Y, Lai S B, Zhou R, Li K, Zhao J B. The high-temperature and high-humidity storage behaviors and electrochemical degradation mechanism of $LiNi_{0.6}Co_{0.2}Mn_{0.2}O_2$ cathode material for lithium ion batteries[J]. J. Power Sources, 2017, 363: 168-176.

[16] Liu S Y, Dang Z Y, Liu D, Zhang C C, Huang T, Yu A S. Comparative studies of zirconium doping and coating on $LiNi_{0.6}Co_{0.2}Mn_{0.2}O_2$ cathode material at elevated temperatures[J]. J. Power Sources, 2018, 396: 288-296.

[17] Yuan J, Wen J W, Zhang J B, Chen D M, Zhang D W. Influence of calcination atmosphere on structure and electrochemical behavior of $LiNi_{0.6}Co_{0.2}Mn_{0.2}O_2$ cathode material for lithium-ion batteries[J]. Electrochim. Acta, 2017, 230: 116-122.

[18] Choi J, Manthiram A. Investigation of the irreversible capacity loss in the layered $LiNi_{1/3}Mn_{1/3}Co_{1/3}O_2$ cathodes[J]. Electrochem. Solid-State Lett., 2005, 8(8): C102-C105.

[19] Hu Q, Wu Y Z, Ren D S, Liao J Y, Song Y Z, Liang H M, Wang A P, He Y F, Wang L, Chen Z H, He X M. Revisiting the initial irreversible capacity loss of $LiNi_{0.6}Co_{0.2}Mn_{0.2}O_2$ cathode material batteries[J]. Energy Stor. Mater., 2022, 50: 373-379.

[20] Hong C Y, Leng Q Y, Zhu J P, Zheng S Y, He H J, Li Y X, Liu R, Wan J J, Yang Y. Revealing the correlation between structural evolution and Li^+ diffusion kinetics of nickel-rich cathode materials in Li-ion batteries[J]. J. Mater. Chem. A, 2020, 8(17): 8540-8547.

[21] Zhou H, Xin F X, Pei B, Whittingham M S. What limits the capacity of layered oxide cathodes in lithium batteries?[J]. ACS Energy Lett., 2019, 4(8): 1902-1906.

[22] Zhao E Y, Fang L C, Chen M M, Chen D F, Huang Q Z, Hu Z B, Yan Q B, Wu M M, Xiao X L. New insight into Li/Ni disorder in layered cathode materials for lithium ion batteries: a joint study of neutron diffraction, electrochemical kinetic analysis and first-principles calculations [J]. J. Mater. Chem. A, 2017, 5(4): 1679-1686.

[23] Chen M M, Zhao E Y, Chen D F, Wu M M, Han S B, Huang Q Z, Yang L M, Xiao X L, Hu Z B. Decreasing Li/Ni disorder and improving the electrochemical performances of Ni-rich $LiNi_{0.8}Co_{0.1}Mn_{0.1}O_2$ by Ca doping[J]. Inorg. Chem., 2017, 56(14): 8355-8362.

[24] Kasnatscheew J, Evertz M, Streipert B, Wagner R, Klopsch R, Vortmann B, Hahn H, Nowak S, Amereller M, Gentschev A C, Lamp P, Winter M. The truth about the 1st cycle coulombic efficiency of $LiNi_{1/3}Co_{1/3}Mn_{1/3}O_2$ (NCM) cathodes[J]. Phys. Chem. Chem. Phys., 2016, 18 (5): 3956-3965.

[25] Wei H X, Tang L B, Huang Y D, Wang Z Y, Luo Y H, He Z J, Yan C, Mao J, Dai K H, Zheng J C. Comprehensive understanding of Li/Ni intermixing in layered transition metal oxides[J]. Mater. Today, 2021, 51: 365-392.

[26] Huang Z J, Wang Z X, Zheng X B, Guo H J, Li X H, Jing Q, Yang Z H. Structural and electrochemical properties of Mg-doped nickel based cathode materials $LiNi_{0.6}Co_{0.2}Mn_{0.2-x}Mg_xO_2$ for lithium ion batteries[J]. RSC Adv., 2015, 5 (108): 88773-88779.

[27] Huang Z J, Wang Z X, Jing Q, Guo H J, Li X H, Yang Z H. Investigation on the effect of Na doping on structure and Li-ion kinetics of layered $LiNi_{0.6}Co_{0.2}Mn_{0.2}O_2$ cathode material[J]. Electrochim. Acta, 2016, 192: 120-126.

[28] Yoon C S, Choi M J, Jun D W, Zhang Q, Kaghazchi P, Kim K H, Sun Y K. Cation ordering of Zr-doped $LiNiO_2$ cathode for lithium-ion batteries[J]. Chem. Mater., 2018, 30(5): 1808-1814.

[29] Liu S Y, Chen X, Zhao J Y, Su J M, Zhang C C, Huang T, Wu J H, Yu A S. Uncovering the role of Nb modification in improving the structure stability and electrochemical performance of $LiNi_{0.6}Co_{0.2}Mn_{0.2}O_2$ cathode charged at higher voltage of 4.5 V[J]. J. Power Sources, 2018, 374: 149-157.

[30] Jo J H, Jo C H, Yashiro H, Kim S J, Myung S T. Re-heating effect of Ni-rich cathode material on structure and electrochemical properties[J]. J. Power Sources, 2016, 313: 1-8.

[31] Noh H J, Youn S, Yoon C S, Sun Y K. Comparison of the structural and electrochemical properties of layered $Li[Ni_xCo_yMn_z]O_2$ (x = 1/3, 0.5, 0.6, 0.7, 0.8 and 0.85) cathode material for lithium-ion batteries[J]. J. Power Sources, 2013, 233: 121-130.

[32] Eom J, Kim M G, Cho J. Storage characteristics of $LiNi_{0.8}Co_{0.1+x}Mn_{0.1-x}O_2$ (x = 0, 0.03, and 0.06) cathode materials for lithium batteries[J]. J. Electrochem. Soc., 2008, 155 (3): A239-A245.

[33] Shen Y B, Wu Y Q, Xue H J, Wang S H, Yin D M, Wang L M, Cheng Y. Insight into the coprecipitation-controlled crystallization reaction for preparing lithium-layered oxide cathodes[J]. ACS Appl. Mater. Interfaces, 2021, 13(1): 717-726.

[34] Shaju K M, Rao G V S, Chowdari B V R. Performance of layered $Li(Ni_{1/3}Co_{1/3}Mn_{1/3})O_2$ as cathode for Li-ion batteries[J]. Electrochim. Acta, 2002, 48(2): 145-151.

[35] Su Y F, Chen G, Chen L, Li W K, Zhang Q Y, Yang Z R, Lu Y, Bao L Y, Tan J, Chen R J, Chen S, Wu F. Exposing the {010} planes by oriented self-assembly with nanosheets to improve the electrochemical performances of Ni-rich $Li[Ni_{0.8}Co_{0.1}Mn_{0.1}]O_2$ microspheres[J]. ACS Appl. Mater. Interfaces, 2018, 10(7): 6407-6414.

[36] Hua W B, Liu W Y, Chen M Z, Indris S, Zheng Z, Guo X D, Bruns M, Wu T H, Chen Y X, Zhong B H, Chou S L, Kang Y M, Ehrenberg H. Unravelling the growth mechanism of hierarchically structured $Ni_{1/3}Co_{1/3}Mn_{1/3}(OH)_2$ and their application as precursors for high-power cathode materials[J]. Electrochim. Acta, 2017, 232: 123-131.

[37] Matienzo L J, Yin L I, Grim S O, Jr S W E. X-ray photoelectron spectroscopy of nickel compounds[J]. Inorg. Chem., 1973, 12: 2762-2769.

[38] Kim K S, Winograd N. X-ray photoelectron spectroscopic studies of nickel-oxygen surfaces using oxygen and argon ion-bombardment[J]. Surf. Sci., 1974, 43(2): 625-643.

[39] Tan B J, Klabunde K J, Sherwood P M A. XPS studies of solvated metal atom dispersed (SMAD) catalysts. Evidence for layered cobalt-manganese particles on alumina and silica[J]. J. Am. Chem. Soc., 1991, 113: 855-861.

[40] Aoki A. X-ray Photoelectron spectroscopic studies on ZnS: MnF_2 Phosphors[J]. Jpn. J. Appl. Phys., 1976, 15: 305-311.

阳离子无序和表面化学残留物对层状氧化物阴极初始库仑效率影响的研究

刘晋利[1,2],吴涵峰[1,3],刘志北[1],吴英强[1*],王　莉[1],卑凤利[2],何向明[1*]

(1. 清华大学, 核能与新能源技术研究院, 北京 100084; 2. 南京理工大学,国家民用爆破器材质量监督检验中心, 江苏 南京 210094; 3. 中国矿业大学, 化学与环境工程学院, 北京 100083)

摘要: 锂层状氧化物 $LiNi_{0.6}Co_{0.2}Mn_{0.2}O_2$(NCM622)是电动汽车高能锂离子电池中最有前途的正极材料之一。然而,目前 NCM622 的一个问题是其初始库仑效率(ICE)只有约 87%,比 $LiCoO_2$ 或 $LiFePO_4$ 至少低 6%。在本工作中,我们研究了在烧结过程中形成的表面化学残留物(如 LiOH 和 Li_2CO_3)和 Li/Ni 阳离子混排对 ICE 的影响。结果表明,当烧结温度从 825 ℃ 提高到 900 ℃ 时,样品的 ICE 从 80.80%提高到 86.68%,而相应的 Li/Ni 阳离子混排和表面化学残留物也有所减少。进一步地,我们使用 HNO_3 溶液洗涤去除 825 ℃ 烧结后的样品的表面残留物,发现尽管 Li/Ni 阳离子紊乱有所增加,但 ICE 提高 3.57%。这些结果表明,通过适当的烧结工艺和后处理技术将表面残留量和 Li/Ni 阳离子混排降至最低是获得高 ICE 并改善 NCM622 电化学性能的关键。

关键词: 锂层状氧化物; 首圈库仑效率; 表面残碱; 锂镍阳离子混排